Electro-optic frequency comb based IPDA lidar: assessment of speckle issues

William Patiño, Nicolas Cezard

Research Article | Vol. 30, No. 10 / 9 May 2022 / Optics Express 15963
Optics EXPRESS

Electro-optic frequency comb based IPDA lidar: assessment of speckle issues

WILLIAM PATIÑO AND NICOLAS CÉZARD*

ONERA/DOTA, Université de Toulouse, F-31055 Toulouse, France
*nicolas.cezard@onera.fr

Abstract: We present a theoretical, numerical and experimental assessment of the impact of speckle on a dual electro-optic frequency comb (EOFC) based system for integrated path differential absorption (IPDA) measurements. The principle of gas concentration measurements in a dual EOFC configuration in the absence of speckle is first briefly reviewed and experimentally illustrated using a C_2H_2 gas cell. A numerical simulation of the system performance in the presence of speckle is then outlined. The speckle-related error in the concentration estimate is found to be an increasing function of the product between the roughness of the backscattering surface and the EOFC line-spacing. As this product increases, the speckle-induced power fluctuations in the comb lines are no longer correlated to each other. To confirm this, concentration measurements are conducted using backscattered light from two different surfaces. Experiment results are in very good agreement with numerical simulations. Though detrimental for IPDA measurements, it is finally shown that decorrelation of speckle noise can be advantageously exploited for surface characterization in a dual EOFC configuration.

1. Introduction

Differential absorption Lidar technology (DIAL) has proven to be a powerful tool for remote sensing of atmospheric trace gases. Traditionally in such systems two laser pulses having slightly different wavelengths are sent to a gas column. Wavelengths are chosen such that one of the pulses is significantly absorbed by the target gas (on-line pulse) and the other is barely absorbed (off-line pulse). By comparison of backscattered signals from a hard surface or atmospheric aerosols, it is possible to estimate the concentration over the target gas column. When a hard surface is used, the technique is usually called integrated-path DIAL (IP-DIAL) or equivalently, integrated path differential absorption (IPDA). Some DIAL lidars also use more than two wavelengths, so as to scan partially or completely the target gas absorption line. For IPDA lidars, it has been shown that this strategy can have significant advantages [1,2] to reduce systematic errors in the gas content measurement, due to possible baseline structures, pressure-induced frequency shifts of the absorption line, or laser frequency drifts.

However, sending two (or more) different wavelengths sequentially in time can also induce some bias on the measurement simply because of the time lag between emitted wavelengths. If the atmosphere is changing quickly or if the lidar platform is moving (vehicle, airplane, satellite, ...), the different wavelengths do not travel exactly through the same atmospheric path, neither do they impact the same surface at the end of the line of sight. Minimizing this time lag generally puts additional technical constrains to the laser emitter. For instance, the future space-borne IPDA lidar MERLIN, designed for methane monitoring with a two-wavelength system, will have a ground spot velocity of 7km/s [3]. This makes mandatory to have a double-pulse laser where the on-line and off-line pulses are very closely emitted (250 µs in this case), which is technically demanding.

In a previous work [4] a new concept has been suggested to perform simultaneous and multi-frequency IPDA measurement of a target gas (namely CO_2) from space. The concept relies on the dual-comb spectroscopy technique (DCS) using electro-optic modulators (EOM); hence the name

#457064 https://doi.org/10.1364/OE.457064
Journal © 2022 Received 24 Feb 2022; revised 26 Mar 2022; accepted 27 Mar 2022; published 25 Apr 2022

Optics EXPRESS

EOFC for electro-optic frequency-comb [5]. This EOFC technique could potentially overcome the two above-mentioned drawbacks by sending simultaneously evenly-spaced frequencies over an absorption line. However, in order to retrieve all the frequency components simultaneously, coherent detection is required. As a consequence, speckle noise from the Earth surface is expected to be a major issue for an EOFC-based spaceborne IPDA lidar. The principle of measuring a gas absorption line and quantifying a gas content using DCS with an EOFC-based emitter has already been demonstrated in previous works [5–14]. However, most of them were conducted in gas cells or using retro-reflectors. Therefore, the impact of speckle on such measurements, with an IPDA lidar perspective, has not been evaluated so far to our knowledge.

This paper examines the impact of speckle noise on the performance of a dual EOFC system for IPDA measurements. Section 2 shortly reviews the principle of DCS using EOFCs in the absence of speckle noise. An experimental setup for gas concentration measurements is presented. The approach used to determine both the gas concentration and the central frequency of the EOFC is discussed. Later, in section 3, we calculate the field of an EOFC backscattered from a rough surface by means of a mathematical model and we derive an expression for the correlation of the speckle-induced power fluctuations in the dual EOFC signals. Then, a numerical simulation of an EOFC-based IPDA system in presence of speckle is presented. We evaluate numerically the influence of the roughness of the backscattering surface on the accuracy of the gas concentration estimate. Experimentally, the influence of speckle correlation on concentration measurements is assessed by comparing measurements conducted over two different backscattering surfaces. Finally, in section 4, the possibility of using a dual EOFC system for surface characterization/discrimination is discussed and a simple experimental setup capable of measuring the roughness of distant surfaces is presented. To the best of our knowledge, this is the first experimental demonstration of a dual-EOFC system exploiting speckle correlation for surface characterization.

2. Gas concentration measurements: all-fiber configuration

As reported in [6], two main configurations for DCS can be distinguished: the symmetric configuration where both frequency combs (FC) are used to probe the sample, and the asymmetric configuration when one FC probes the sample and the other one acts as a local oscillator (LO). The latter is more attractive for lidar measurements since the LO can be used to amplify the lidar signal which is significantly attenuated. Therefore we shall only discuss the asymmetric configuration in this paper.

2.1. Electro-optic dual comb spectroscopy

An asymmetric experimental setup for DCS is presented in Fig. 1. The laser signal is split into two arms and one of them is frequency-shifted by an acousto-optic modulator (AOM) for heterodyne detection. The probe EOFC and the LO EOFC are produced by means of an EOM in each arm of the interferometer. The generated EOFCs are also split into two branches. One branch of the probe EOFC is sent to a gas cell and recombined on a photodetector (PD-1) with one of the branches of the LO EOFC to produce a measurement beat signal s_m. The other branch, which does not interact with the sample, is also recombined with the LO EOFC on a second photodetector (PD-2) in order to generate a reference beat signal s_{ref}. Assuming an odd number N of comb lines, we can write the electric field of the EOFCs as [15]:

$$E_X(t) = E_{0,X} \sum_{n=-\frac{N-1}{2}}^{n=\frac{N-1}{2}} |a_{X,n}| \exp[i(\omega_{0,X} + n\omega_{M,X})t] \exp(i\phi_{X,n}) + c.c. \quad (1)$$

where $\omega_{0,X} = 2\pi\nu_{0,X}$ and $\omega_{M,X} = 2\pi f_{M,X}$, with $\nu_{0,X}$ the carrier frequency of the EOFC and $f_{M,X}$ its line-spacing, given by the driving frequency of the EOM. The subindex $_X$ stands for $_P$ (probe)

Optics EXPRESS

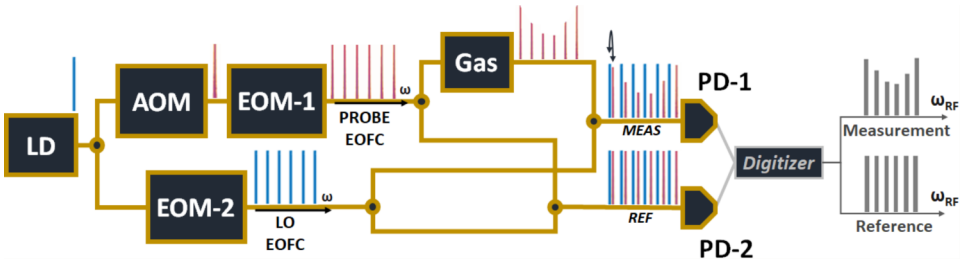

Fig. 1. All-fiber experimental setup for DCS using EOFCs. EOM-1 generates the probe EOFC (red comb) which is absorbed by the gas sample and recombined with the LO EOFC (blue comb) to produce a measurement RF comb. A reference RF comb is also generated. Both signals are digitized and filtered before processing. LD, laser diode; AOM, acousto-optic modulator; EOM, electro-optic modulator; Gas, C_2H_2 cell; PD, photodetector.

and $_{LO}$ (local oscillator). n is the comb line index. $|a_{X,n}|$ and $\phi_{X,n}$ are respectively the amplitude and phase distributions of the EOFCs.

The complex amplitude transmission of the gas sample can be written as: $a_T(\omega) = \exp[-\tau(\omega)/2 - i\varphi(\omega)]$, where $\tau(\omega)$ is the optical depth and $\varphi(\omega)$ the phase shift. If we define $\Delta\omega_M = |\omega_{M,P} - \omega_{M,LO}|$, then the beat frequencies can be written as: $\omega_{n,RF} = \omega_A + n\Delta\omega_M$. Where $\omega_A = 2\pi f_A$, with f_A the driving frequency of the AOM. After recombination and low-pass filtering, the measurement beat signal is [15]:

$$s_m \propto \sum_{n=-\frac{N-1}{2}}^{n=\frac{N-1}{2}} |a_{P,n}||a_{LO,n}| \cos[\omega_{n,RF}t - \varphi(\omega_{n,P}) + \Delta\phi_n] \times \exp[-\tau(\omega_{n,P})/2] \tag{2}$$

where $\omega_{n,P} = \omega_{0,P} + n\omega_{M,P}$ are the probe frequencies. In the spectral domain, the measurement signal corresponds to a N-line comb lying in the radio-frequency (RF) range, which have been attenuated and phase shifted by the complex amplitude transmission profile of the gas sample at the probe frequencies $\omega_{n,P}$. In the same way, the reference beat signal corresponds to a N-line comb in the RF domain. The RF combs line-spacing is given by: $\Delta f_M = |f_{M,P} - f_{M,LO}|$. The transmission profile of the sample at the probe frequencies is calculated by comparing the power and/or the phase distributions of the measurement RF comb to those of the reference RF comb. This type of measurement relies on the stability and mutual coherence of the EOFCs. The term $\Delta\phi_n$ accounts for the phase difference between the probe and the LO EOFCs. It acts as an offset for the phase profile measurement.

2.2. Concentration estimation

In DCS, the powers of RF comb lines are calculated in the frequency domain. This is done by integrating the power spectra around the beat frequencies $\omega_{n,RF}$. Then, the experimental power ratio R_{exp} between the measurement RF comb and the reference RF comb can be written as:

$$R_{exp}(\omega_{n,RF}) = \frac{\int_{\omega_{n,RF}-\frac{\Delta w}{2}}^{\omega_{n,RF}+\frac{\Delta w}{2}} |\hat{s}_m(\omega)|^2 d\omega}{\int_{\omega_{n,RF}-\frac{\Delta w}{2}}^{\omega_{n,RF}+\frac{\Delta w}{2}} |\hat{s}_{ref}(\omega)|^2 d\omega} \tag{3}$$

where Δw is the integration window size and $\hat{s}$ denotes the Fourier transform of the signals. This experimental measurement is related to the transmission profile of the gas sample T_{gas} by: $R_{exp}(\omega_{n,RF}) = L \times T_{gas}(\omega_{n,P}) + O$. Where L is a scaling factor and O a residual transmission offset.

Optics EXPRESS

These coefficients account for the differential losses between the reference and the measurement arms.

In the case of dual EOFC signals, we can write the carrier-to-noise ratio (CNR) of the n-th RF comb line as:

$$\mathrm{CNR}_{X,n} = \frac{\int_{\omega_{n,RF}-\Delta w/2}^{\omega_{n,RF}+\Delta w/2} |\hat{s}_X(\omega)|^2 d\omega}{\int_{\omega_{n,RF}-\Delta w/2}^{\omega_{n,RF}+\Delta w/2} |\hat{s}_{X,noise}(\omega)|^2 d\omega} - 1 \tag{4}$$

where the subindex $_X$ denotes $_m$ (measurement) and $_{ref}$ (reference). $|\hat{s}_{noise}(\omega)|^2$ is the noise power spectrum given by the dominant noise source (typically shot-noise or detection noise). The CNR will be used later in the paper to evaluate and compare the quality of dual EOFC signals.

On the other hand, the optical depth of the sample is given by $\tau(\omega) = p_c\sigma(\omega)$. Where $p_c = \mathrm{VMR}l_c$ is the concentration parameter in units of ppm.m, l_c is the length of the gas column and VMR the volume mixing ratio of the gas species in ppm. $\sigma(\omega) = 10^{-6}\sigma_0(\omega)n_a$ is the scaled cross section of the gas in units of $\mathrm{ppm}^{-1}.m^{-1}$ with n_a the air number density and $\sigma_0(\omega)$ the cross section in m^2.

After computing the power ratio R_{exp}, the measured optical depth τ_n is given by:

$$p_c\sigma(\omega_{n,P}) = -\log[\frac{R_{exp}(\omega_{n,RF}) - O}{L}] \tag{5}$$

This can be interpreted as a multi-frequency Beer-Lambert equation as n varies from -$(N-1)/2$ to $(N-1)/2$. In order to estimate the concentration parameter p_c, we must know the additional parameters affecting the measurement: L, O and the probe frequencies $\omega_{n,P}$. Indeed their values are dependent on experimental conditions: detector noise level, detector responsivity, polarization-related losses, losses in the modulators, current and temperature of the laser diode. The latter have a direct impact on the frequency of the laser signal and thus can significantly modify the probed cross section.

For a given gas species and a known pressure and temperature, the scaled cross section is known and can be computed using the high-resolution transmission (HITRAN) database. Using the fact that all the frequencies in the probe EOFC are equally-spaced (by $\omega_{M,P}$) and absorbed simultaneously by the gas sample, it is possible to solve Eq. (5) using an inversion method, for instance, a least squares optimization. The solution yields an estimation of the concentration parameter, as well as the additional parameters: the scaling factor L, the residual transmission offset O and the central frequency of the probe EOFC $\omega_{0,P}$. The mean gas concentration along the optical path can be computed provided that its length is known. The estimation of L and O allows to compensate power fluctuations common to all the comb lines, without degrading the concentration measurement. The possibility of estimating the central frequency $\omega_{0,P}$ from experimental data makes the dual EOFC system robust to laser frequency drifts.

2.3. Experiment results

Following the experimental setup outlined in Fig. 1, we conducted concentration measurements of a pure, low pressure (50 Torr), C_2H_2 gas cell of 16.5 cm in length. The P-23 (1539.42975nm) absorption feature was probed with an EOFC generated by means of an electro-optic phase modulator and a distributed feedback LD. The probe EOFC line-spacing was set to 200MHz and the LO EOFC line-spacing to 201MHz. A 40 MHz AOM was used to shift the frequency of the probe EOFC. The modulation indices of EOM-1 and EOM-2 were set to m_1=1.7 and m_2=2.9 respectively, so as to retrieve a reference RF comb having 5 lines with a comparable power.

Figure 2 (left) shows the spectra of the measurement and reference beat signals. As expected, spectra are centered around 40MHz and the RF comb lines are separated by Δf_M=1MHz. We observe that the central lines (39, 40, 41MHz) of the measurement comb are attenuated with

Optics EXPRESS

respect to the reference comb due to absorption of the gas sample. Detector noise is the dominant noise source, resulting in a mean CNR of 10^4, for both the measurement and the reference signals. The error in the optical depth measured by the n-th RF comb line is given by [16]: $\Delta(\tau_n) = \sqrt{1/\mathrm{CNR}_{m,n} + 1/\mathrm{CNR}_{ref,n}}$. Since there is no delay between the arms of the interferometer, the observed linewidth does not correspond to laser phase noise but to phase noise added by the RF driving signals of the EOMs. As discussed in [5], this noise increases linearly with the comb line index n. The full width half maximum (FWHM) of the RF comb lines is limited by the RF resolution of 25kHz (given by the short acquisition time of 40μs).

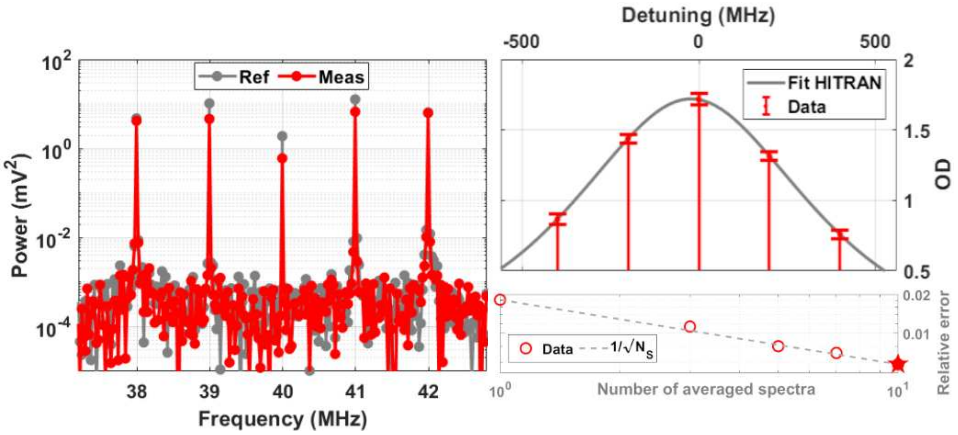

Fig. 2. (Left) Measurement RF comb and reference RF comb. The measurement RF comb was scaled for comparison with the reference RF comb. (Top right) Fit of the average measured optical depth (OD) to the HITRAN (2008 version; P-23 line of C_2H_2) profile. Error bars correspond to the standard deviation of the optical depth before averaging. (Bottom right) Relative error in the concentration parameter estimate as a function of the number of averaged spectra.

150 beat signals of 40μs were recorded at a rate of 15 signals per second. The power spectra were computed and averaged in groups of consecutive signals. Then the power ratio between the measurement RF comb and the reference RF comb was calculated using an integration window of $\Delta w = 0.1$MHz. The concentration parameter was estimated along with the central frequency of the probe EOFC $\omega_{0,P}$ and the linear coefficients L and O using a weighted least squares optimization. The weights were given by the inverse of the variance (computed from experimental data) associated to each measurement point. Figure 2 (top right) presents the fit of the average optical depth to the HITRAN profile. After averaging over groups of 10 spectra, it was possible to estimate the concentration parameter with a relative error of 0.6% and to determine the central frequency of the probe EOFC with an accuracy of 2MHz; the error being the standard deviation of the estimates. This result is presented in Fig. 2 (bottom right -star marker-) which shows the error in the concentration parameter p_c as a function of the number of averaged spectra. As expected, the relative error in the gas concentration decreases as $1/\sqrt{N_S}$, with N_S being the number of averaged spectra.

3. Assessment of speckle issues

Coherent lidars collect light backscattered from distant objects which then interferes with a LO in a detector. Speckle fluctuations are an important source of noise in such systems; they become the dominant noise source for coherent systems having a CNR $\gg 1$. If a time-varying backscattering surface is considered, the power of the measured beat signal can be treated as

Optics EXPRESS

an exponential random variable [16,17]. For this reason, in coherent IPDA lidar systems, a large number of independent measurements must generally be averaged in order to guarantee an accurate estimation of the gas concentration [18].

In a dual EOFC lidar system, the probe EOFC is absorbed by the target gas, backscattered by a distant surface and recombined with the LO EOFC to generate a measurement beat signal on a PD. In such system each frequency component in the probe EOFC is affected by speckle noise. Thus, the powers of the measurement RF comb lines follow as well a negative exponential distribution; hence, their standard deviations equal their mean values. Since all the frequency components are backscattered simultaneously, speckle-induced fluctuations can be correlated to a certain extent. We aim to determine under which conditions the speckle noise affecting the measurement is spectrally correlated, i.e., the speckle-induced power fluctuations in the measurement RF comb lines are correlated to each other.

Correlation of speckle noise is important for gas concentration measurements since it determines the number of independent signals required to perform an accurate estimate. Speckle correlation has been deeply studied by Goodman [19] and Parry [20,21]. The effects of speckle correlation on direct detection IPDA lidar systems can be found in [22,23]. In this section we examine the impact of speckle noise on the structure of the measurement RF comb and its implications for trace gas concentration measurements.

3.1. Speckle decorrelation and comb distortion

Using Goodman's approach (see [17], Eq. (2.4)), we can write the electric field of the backscattered probe EOFC at an observation point far from the scattering surface as:

$$E_{\mathrm{BS}} = E_{0,P} \sum_{n=-\frac{N-1}{2}}^{n=\frac{N-1}{2}} C_n \, |a_{P,n}| \exp[i(\omega_{0,P} + n\omega_{M,P})t] \exp(i\phi_{P,n}) + c.c. \tag{6}$$

$$C_n = \sum_{k=1}^{K} \frac{|A_k|}{\sqrt{K}} \exp[\frac{i(\omega_{0,P} + n\omega_{M,P})2z_k}{c}] \tag{7}$$

We observe that the backscattered field equals the incoming probe EOFC, with the comb lines modulated by the complex coefficients C_n. We assumed that the rough surface is composed of K distant scatterers. The scatterers are distributed on the surface plane with depth deviations given by the random variable Z. Each scatterer modulates the amplitude of the incoming field by a factor $|A_k|$ and introduces a phase shift of $\frac{(\omega_{0,P}+n\omega_{M,P})2z_k}{c}$ to the n-th EOFC line.

The coefficients C_n can be associated with the amplitude of a speckle field, far from the scattering surface, produced by an incident electric field of frequency $\omega_{0,P} + n\omega_{M,P}$ and unit amplitude. We assume that the roughness of the surface is much larger than the carrier wavelength; therefore the coefficients C_n correspond to a random walk in the $[-\pi, \pi]$ interval [17]. It follows that the mean of the modulation coefficients is zero. After recombination with the LO EOFC, the amplitudes of the measurement RF comb lines are modulated by the coefficients C_n as well.

Using Goodman's result for the correlation coefficient of two speckle fields produced by different frequency components (see [19], Eq. (6.5)), it is straightforward to calculate the correlation of the complex coefficients C_n and $C_{n'}$ associated to two EOFC lines of frequency $\omega_{0,P} + n\omega_{M,P}$ and $\omega_{0,P} + n'\omega_{M,P}$ respectively. We obtain:

$$\rho(C_n, C_{n'}) = \Phi_Z[\frac{\omega_{M,P}\Delta n}{\pi c}] \tag{8}$$

With $\Delta n = n - n'$ the comb line index difference and Φ_Z the characteristic function of the random variable Z, i.e., the inverse Fourier transform of the probability density function (PDF) $f_Z(z)$.

Optics EXPRESS

If we describe the surface deviations as a Gaussian zero-mean random variable with standard deviation σ_z (surface roughness), then the correlation of the complex modulation coefficients is given by:

$$\rho(C_n, C_{n'}) = \exp[-\frac{1}{2}(\sigma_\phi \Delta n)^2] \tag{9}$$

With $\sigma_\phi = \frac{2\omega_{M,P}\sigma_z}{c}$. We note that the correlation of the complex amplitude of the EOFC lines after backscattering decreases as a Gaussian function of the line spacing Δn. It follows that the correlation of the RF comb lines power varies as $\exp[-(\sigma_\phi \Delta n)^2]$ (see [17]). The width of the correlation function is inversely proportional to σ_ϕ.

Decorrelation of the speckle-induced power fluctuations results in a distortion of the measurement RF comb structure. Thus, if we intend to preserve the RF comb structure after backscattering from a rough surface, the line-spacing of the probe EOFC should be adjusted according to the surface roughness in order to maximize the width of the correlation function.

3.2. Concentration measurements in presence of speckle: numerical simulations

An EOFC based IPDA lidar will be inevitably constrained by speckle noise, and the structure of the measurement RF comb will be distorted to some extent, depending on the experimental parameters. In this section we present a numerical simulation of dual EOFC signals in the presence of speckle.

We simulated a total of 10^3 DCS signals of a C_2H_2 low pressure gas cell in presence of speckle for 2 different surface roughness, i.e., 2 values of the parameter σ_ϕ. The simulated EOFCs were assumed to be generated out of the same laser signal by means of a pair of identical phase modulators. The rough surface was described as a collection of 100 scatterers following a centered Gaussian distribution of standard deviation σ_z. The field of the backscattered probe EOFC was found by coherent sum of the field reflected by each scatterer on the surface as indicated in Eq. (6). The cases of a measurement in the absence of speckle, a completely correlated speckle ($\sigma_\phi \approx 0$) and a totally uncorrelated speckle noise ($\sigma_\phi \gg 1$) were also simulated.

As σ_ϕ increases, the structure of the measurement RF comb is more and more distorted due to speckle decorrelation. For $\sigma_\phi \approx 1$, the correlation coefficient of the power of adjacent comb lines ($|\Delta n| = 1$) equals to $1/e$. Figure 3 illustrates the spectral distortion of the measurement RF comb for $\sigma_\phi = 0.4$. We observe that the powers of the measurement RF comb lines are randomly modulated with respect to the reference RF comb. The absorption profile of the gas is no longer distinguishable as it was in the case without speckle. Averaging independent measurements is hence required to perform an accurate estimation of the gas concentration.

The power spectra of the simulated signals were computed and averaged over a variable number N_S of independent spectra before calculating the power ratio in Eq. (4). Only the 5 strongest RF comb lines were taken into account. The scaling factor and the concentration parameter were reiteratively estimated using the maximum-likelihood (ML) method. The remaining parameters were fixed to their input values. The covariance matrix used for the ML estimation was computed from simulated data. Figure 4 shows the relative error in the estimated concentration as a function of the number of averaged spectra for the different values of σ_ϕ. The simulation took into account Gaussian white detection noise of the signals resulting in a mean detection-noise-limited CNR of about 10^3 for both the measurement and the reference signals. The error in the concentration estimate was calculated as the standard deviation of 100 different estimates.

We observe that for all values of σ_ϕ, the error decreases as the number of averaged spectra N_S increases. For a fixed N_S, the relative error is an increasing function of σ_ϕ. Thereby, the impact of speckle on concentration measurements is to increase the number of required averages in order to achieve a given precision. No bias in the concentration estimate due to speckle was observed. The estimates approach the $1/\sqrt{N_S}$ trend as N_S increases regardless of the value of σ_ϕ. In the case of a completely correlated speckle noise, the measured profile is not distorted, and the only

Optics EXPRESS

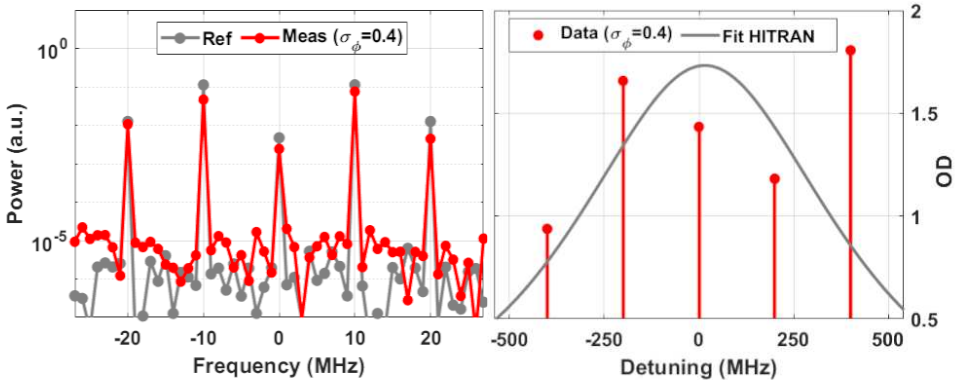

Fig. 3. (Left) Simulated measurement and reference RF combs in the presence of speckle before averaging for $\sigma_\phi = 0.4$. Spectral distortion of the measurement RF comb with respect to the reference RF comb is observed. (Right) Optical depth calculated from the distorted RF comb.

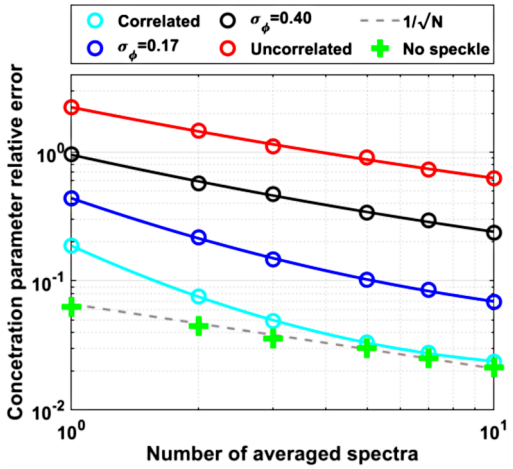

Fig. 4. Simulated relative error in the concentration parameter estimate as a function of the number N_S of averaged spectra for different values of σ_ϕ. The dashed line indicates the $1/\sqrt{N_S}$ evolution. The cases of a totally correlated speckle noise ($\sigma_\phi \approx 0$) and a fully uncorrelated speckle ($\sigma_\phi \gg 1$) are presented. The simulation includes detection noise resulting in a mean CNR of around 10^3 for the no speckle case.

Optics EXPRESS

consequence of speckle is a random modulation of the measurement signal total power. Then, in that case, the relative error approaches the one without speckle as the number of averaged spectra increases.

3.3. Experiment results

With the purpose of experimentally validating the results above, concentration measurements of a low pressure C_2H_2 gas cell were performed using light backscattered from two different surfaces. The setup is outlined in Fig. 5 (dashed and continuous lines). The probe EOFC was absorbed by a C_2H_2 gas cell, amplified by an Erbium-doped fiber amplifier (EDFA), collimated and backscattered by a distant vibrating surface located 1m from the fiber collimator. The diameter of the laser spot on the target surface was 5mm ($1/e^2$). The backscattered signal was then coupled into a single mode polarization maintaining optical fiber and recombined with a branch of the LO EOFC on a PD. The coupling, propagation and scattering losses amount to approximately 70dB. The surface vibration ensured renewal of speckle noise; this allowed to record a high number of independent signals in a short time. Vibrations were induced by a speaker coupled to the backscattering surface. Two different backscattering surfaces were studied: a flat cardboard (surface-1: σ_z<1mm) and a slice of corrugated polystyrene (surface-2: $\sigma_z \approx 1cm$).

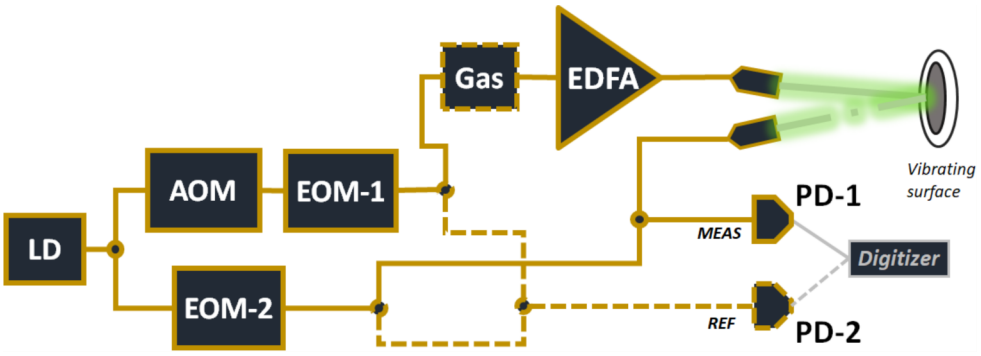

Fig. 5. Experimental setup for gas concentration measurements in the presence of speckle (continuous and dashed lines) and surface characterization (continuous lines). For concentration measurements, the gas sample is located before the Erbium-doped fiber amplifier (EDFA) and both the LO EOFC and the probe EOFC are split into two branches in order to generate the reference beat signal. A dynamic speckle is obtained by means of a speaker attached to the backscattering surface.

The line-spacing of the probe EOFC was set to $f_{M,P}$=386MHz in order to cover the C_2H_2 absorption feature (P-23) and observe a significant decorrelation of the speckle-induced power fluctuations. Due to a variable Doppler shift, resulting from the vibration of the backscattering surface, the beat frequencies oscillated with an amplitude of about 0.8MHz. Thus, in order to distinguish the different RF comb lines, the LO EOFC line-spacing was fixed to $f_{M,LO}$ =380MHz, yielding Δf_M=6MHz.

We performed 3 concentration measurements for both surfaces. For each measurement, 500 beat signals of 50µs were acquired at a rate of 15 signals per second. Due to a different surface reflectance, the mean CNR was slightly higher for surface-1 than for surface-2. To mitigate this difference, we selected around 350 signals having approximately the same CNR (in the order of 10^3) for proper comparison of both surfaces, as illustrated in Fig. 6 (left). Figure 6 (right) presents the fit of the average optical depth to the HITRAN profile for a measurement conducted using surface-2. Measurements for both surfaces were limited by speckle noise. The error in the measured optical depth is hence given by [16]: $\Delta(\tau_n) = \sqrt{(1 + 1/\mathrm{CNR}_{m,n}) + 1/\mathrm{CNR}_{ref,n}}$ since

Optics EXPRESS

only the measurement RF comb is affected by speckle noise. Therefore, the random error in the measured optical depth $\Delta\tau_n \approx 1$ (before averaging), for all the comb lines, regardless of their mean power. After averaging this error is reduced by a factor of $\sqrt{N_S}$.

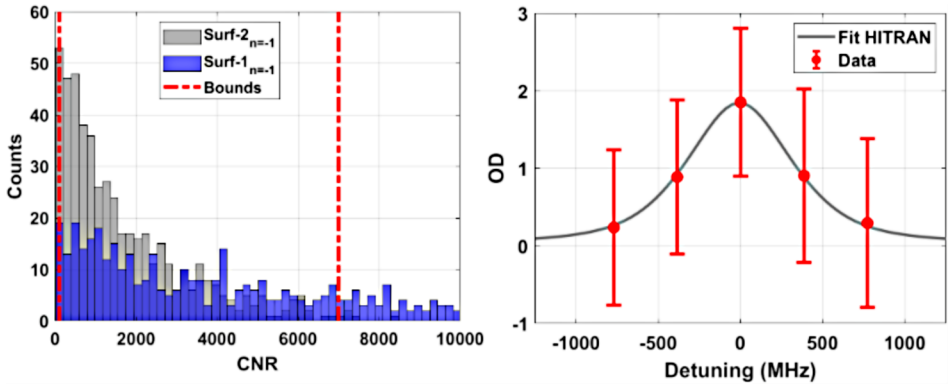

Fig. 6. (Left) CNR of the $_{n=-1}$ measurement RF comb line for both surfaces. The dashed lines indicate CNR bounds used to select data having a comparable CNR. (Right) Fit of the average measured optical depth to the HITRAN profile using light backscattered from surface-2. The error bars correspond to the measured optical depth standard deviation before averaging.

Following the same approach of section 3.2, the selected spectra were averaged over groups of N_S signals. For each measurement, an iterative ML estimation of only the scaling factor and the concentration parameter was performed. The fluctuations of the central frequency of the EOFC were assumed to be negligible during the measurement time (around 30s). Figure 7 shows the relative error in the concentration parameter as a function of the number of averaged spectra N_S for both surfaces. We observe that the measurements using surface-2 present a level of error around 3 times higher compared to the measurements over surface-1, for 10 averaged spectra. Using the results of section 3.1, it is possible to calculate the parameter σ_ϕ for both surfaces (see section 4). For surface-1, we obtain $\sigma_{\phi,1} = 0.01$, which corresponds to an almost completely correlated speckle noise (correlation coefficients above 0.99). For surface-2, we obtain $\sigma_{\phi,2} = 0.17$. If we refer to the simulated results in Fig. 4, we observe that for those same values of σ_ϕ and an equivalent mean CNR, the error levels also differ by a factor of 3, for 10 averaged spectra.

This experiment validates the numerical and theoretical results presented above and it highlights the influence of speckle noise on a EOFC based lidar system. Although the precision of the concentration estimate may vary depending on the selected inversion method, speckle decorrelation represents a physical constraint of any EOFC-based IPDA system.

For an atmospheric EOFC-based IPDA lidar, the line-spacing of the EOFC will be constrained by the width of the gas target absorption feature, typically in the order of 10GHz (FWHM). In addition, the system is expected to perform accurate measurements over any kind of backscattering surface. As an illustration, for a line-spacing of 500MHz and a surface roughness of 0.1m, $\sigma_\phi \approx 2$. Hence, in the most general case, the system would work under conditions of highly uncorrelated speckle noise.

Optics EXPRESS

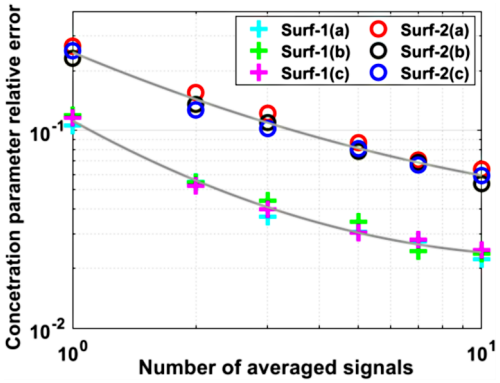

Fig. 7. Relative error in the concentration estimate as a function of the number of averaged spectra for two different surfaces. 3 acquisitions were performed over each surface. Continuous lines represent a quadratic fit in logarithmic scale.

4. Surface characterization

The possibility of using speckle correlation for surface roughness measurements has been explored and demonstrated for decades [24,25]. Furthermore, results of section 3.1 suggest that correlation of speckle noise in a dual EOFC system can be exploited for surface characterization. In principle, if we measure experimentally $\rho(\Delta n)$, it would be possible, by applying a Fourier transform, to retrieve the PDF $f_Z(z)$ of the surface roughness (see Eq. (8)).

In a dual EOFC configuration, in which the probe EOFC is backscattered by the surface and then interferes with the LO EOFC, it is possible to measure the correlation $\rho(\Delta n)$ for different values of Δn. This means that with a simple experimental setup, we could completely characterize the PDF of the surface roughness. Such a setup would be highly tunable, since the correlation function scales with the probe EOFC line-spacing $f_{M,P}$ (see Eq. (9)).

To validate this possibility, a numerical simulation was conducted following the same approach presented in section 3.2. We studied the correlation of the speckle-induced fluctuations in the RF comb lines power as a function of the surface roughness σ_z in the absence of gas absorption. Correlation coefficients were calculated out of 100 simulated signals for 5 different values of σ_z. Results are presented in Fig. 8 as a function of the dimensionless parameter σ_ϕ. As expected, a Gaussian fit allowed to retrieve the roughness of the simulated surface. Simulated results are in very good agreement with theory.

4.1. Experimental demonstration

The possibility of characterizing distant surfaces was also experimentally validated. The setup for surface characterization is depicted in Fig. 5 (continuous lines). We used the same backscattering surfaces presented in section 3.3. The gas cell was removed from the setup and the line-spacings of the EOFCs were varied from 200MHz up to 3GHz, keeping Δf_M = 6MHz. In this configuration there is no need of a reference signal, since we intend to measure the correlation of the speckle-induced power fluctuations in the measurement RF comb.

The powers of the resulting RF comb lines were calculated from 500 segments of 50µs, for 5 different values of the EOFCs line-spacings. Then, the correlation coefficients were computed from experimental data. Results are presented in Fig. 9.

A minor decay in the correlation coefficients is observed as we increase the EOFCs line-spacings for surface-1. A Gaussian fit is performed for a modulation frequency of 1,2 and 3GHz. We obtain a mean surface roughness of $\sigma_{z,1} = 0.6mm$ with a standard deviation of $\Delta\sigma_{z,1} = 0.1mm$.

Optics EXPRESS

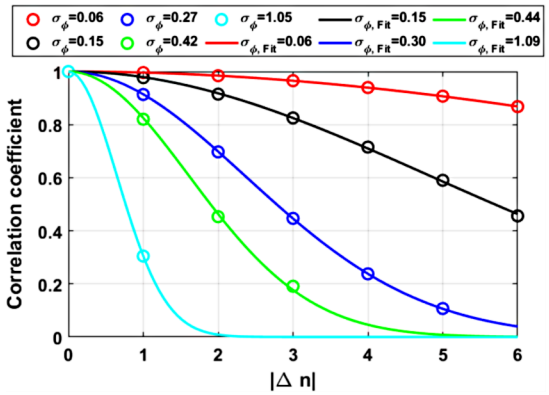

Fig. 8. Simulated correlation coefficients of the RF comb lines power as a function of the line index difference $|\Delta n|$ for 7-line EOFCs. Coefficients were calculated out of 100 simulated signals for 5 values of σ_ϕ and all possible $|\Delta n|$ were taken into account. It was possible to retrieve the roughness of the simulated surface from the fit parameter.

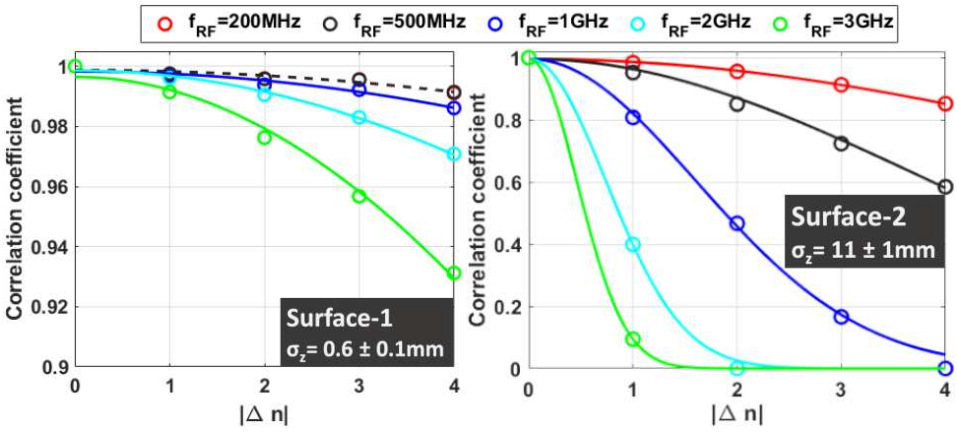

Fig. 9. Correlation coefficients between the powers of the RF comb lines for two different surfaces (cardboard -left- and corrugated polystyrene -right-) as a function of the line-index difference $|\Delta n|$. The line-spacings of the EOFCs were increased from 200MHz up to 3GHz, keeping Δf_M = 6MHz. A Gaussian fit (continuous lines) allowed to estimate the surfaces roughness.

Optics EXPRESS

For surface-2, we note a significant decay in the correlation coefficients. A Gaussian fit allows to estimate the surface roughness. A mean roughness of $\sigma_{z,2} = 11mm$ with a standard deviation of $\Delta\sigma_{z,2} = 1mm$ is found, which is consistent with direct visual observations of the surface. For both surfaces, the Gaussian model fits data very well, thus the assumption of a Gaussian-distributed surface depth is appropriate.

As a final demonstration of the potential of this technique, we implemented a surface discrimination experiment. Using the same setup shown in Fig. 5 (continuous lines), we replaced the vibrating surface by a test surface consisting of a polyurethane foam stuck to a sheet of white paper (see Fig. 10-top-). The test surfaced was swept perpendicularly to the laser beam. The line-spacings of the probe and LO EOFCs were set to 3.005GHz and 3GHz respectively. The powers of the RF comb lines were recorded for two minutes at a rate of around 80 measurements per second.

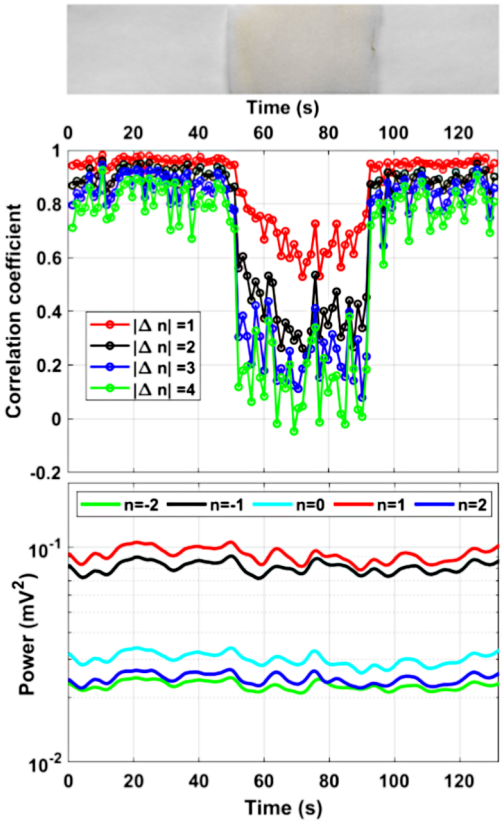

Fig. 10. (Top) Photo of the test surface. (Middle) Correlation coefficients of the powers of the RF comb lines as a function of time for different values of $|\Delta n|$. (Bottom) Average powers of the RF comb lines.

Correlation coefficients of the RF comb lines power as a function of $|\Delta n|$ are shown in Fig. 10 (middle). A significant decay in the correlation coefficients is observed as soon as the laser impacts the foam. The correlation coefficients were calculated out of groups of 100 measurements, which results in one correlation measurement every 1.25s. Figure 10 (bottom) presents the powers of the RF comb lines averaged over a Gaussian window of 9s. We observe no significant variations on the backscattered signal level as the laser impacts the test surface. Results evidence that this technique can be used to discriminate dynamic targets having similar reflectance at the

Optics EXPRESS

working wavelength. This experiment is inline with theoretical expectations and it corroborates the potential of the dual EOFC technique for surface characterization.

5. Conclusion

The impact of speckle on an EOFC-based IPDA system has been assessed from a theoretical and experimental point of view. Firstly, an all-fiber setup for gas concentration measurements using EOFCs was presented. The concentration of a C_2H_2 gas cell (without speckle) was estimated with an error of 0.6% and the central frequency of the EOFC was determined with an accuracy of 2MHz. Then, the theoretical aspects of speckle effects on dual EOFC signals were discussed and a numerical simulation was outlined. The error in the concentration measurement was found to depend on the dimensionless parameter σ_ϕ, which relates the roughness of the backscatterer and the EOFC line-spacing. Numerical simulations illustrated that the structure of the measurement RF comb is distorted as σ_ϕ increases. This distortion results from the decorrelation of the power fluctuations induced by speckle in the measurement RF comb. Speckle-induced power fluctuations are not expected to introduce any systematic error in the measurement.

An experimental setup for gas concentration measurements in a dual EOFC configuration using backscattered light was implemented. Results obtained using two different backscattering surfaces were compared. Measurements for both surfaces were limited by speckle noise. However, the error in the concentration estimate was considerably smaller for the smoother surface, since the speckle-induced fluctuations exhibited a higher correlation. An excellent agreement between numerical simulations and experiment results was observed. An EOFC-based IPDA lidar system designed for atmospheric gas monitoring is expected to work in a regime of strongly uncorrelated speckle noise.

The use of two different PDs and different electronics (amplifiers, filters, ...) is likely to limit the long-term stability of the concentration measurement and may introduce systematic errors. Future works, with a view to developing an EOFC based instrument for remote sensing of atmospheric gases, can be improved by making use of only one detector. This can be achieved, for instance, by adding an extra AOM to frequency shift one of the arms of the interferometer or by working in a pulsed mode of operation.

It is worth noting that the coupling between the surface roughness and the measurement comb structure can be exploited for surface characterization. Theoretical derivations show that the PDF of the surface deviations can be estimated by using a simple dual EOFC setup. Two experimental demonstrations of surface characterization exploiting correlation of speckle noise in a dual EOFC system have been presented, confirming theoretical expectations. These results may open the way for new concepts of compact and tunable surface profilometry devices.

Funding. Office National d'Etudes et de Recherches Aérospatiales (Research contract 51/19282, TELEMAC); Centre National d'Études Spatiales (51/19282); Université de Toulouse (TESS BOOSTER).

Acknowledgments. We gratefully acknowledge the help provided by Philippe Hébert (CNES) for his valuable discussions and François Lemaître (ONERA) for his suggestions and for the borrowed equipment.

Disclosures. The authors declare no conflicts of interest.

Data availability. Data underlying the results presented in this paper are not publicly available at this time but may be obtained from the authors upon reasonable request.

References

1. J. R. Chen, K. Numata, and S. T. Wu, "Error reduction in retrievals of atmospheric species from symmetrically measured lidar sounding absorption spectra," Opt. Express **22**(21), 26055–26075 (2014).
2. H. Riris, M. Rodriguez, J. Mao, G. Allan, and J. Abshire, "Airborne demonstration of atmospheric oxygen optical depth measurements with an integrated path differential absorption lidar," Opt. Express **25**(23), 29307–29327 (2017).
3. G. Ehret, P. Bousquet, C. Pierangelo, M. Alpers, B. Millet, J. B. Abshire, H. Bovensmann, J. P. Burrows, F. Chevallier, P. Ciais, C. Crevoisier, A. Fix, P. Flamant, C. Frankenberg, F. Gibert, B. Heim, M. Heimann, S. Houweling, H. W. Hubberten, P. Jöckel, K. Law, A. Löw, J. Marshall, A. A. Panareda, S. Payan, C. Prigent, P. Rairoux, T. Sachs,

Optics EXPRESS

M. Scholze, and M. Wirth, "MERLIN: A French-German space lidar mission dedicated to atmospheric methane," Remote Sens. **9**(10), 1052 (2017).
4. P. J. Hébert and F. Lemaître, "SCALE: validations and prospects for a novel type of sounding lidar using short frequency combs," *Proc. SPIE 11180, International Conference on Space Optics — ICSO 2018*, 111801T (12 July 2019).
5. A. Parriaux, K. Hammani, and G. Millot, "Electro-optic frequency combs," Adv. Opt. Photonics **12**(1), 223–287 (2020).
6. I. Coddington, N. Newbury, and W. Swann, "Dual-comb spectroscopy," Optica **3**(4), 414–426 (2016).
7. D. A. Long, A. J. Fleisher, K. O. Douglass, S. E. Maxwell, K. Bielska, J. T. Hodges, and D. F. Plusquellic, "Multiheterodyne spectroscopy with optical frequency combs generated from a continuous-wave laser," Opt. Lett. **39**(9), 2688–2690 (2014).
8. P. Martin-Mateos, M. Ruiz-Llata, J. Posada-Roman, and P. Acedo, "Dual-comb architecture for fast spectroscopic measurements and spectral characterization," IEEE Photonics Technol. Lett. **27**(12), 1309–1312 (2015).
9. P. Martín-Mateos, B. Jerez, P. Largo-Izquierdo, and P. Acedo, "Frequency accurate coherent electro-optic dual-comb spectroscopy in real-time," Opt. Express **26**(8), 9700–9713 (2018).
10. A. Fleisher, D. Long, Z. Reed, J. Hodges, and D. Plusquellic, "Coherent cavity-enhanced dual-comb spectroscopy," Opt. Express **24**(10), 10424–10434 (2016).
11. P. Guay, J. Genest, and A. Fleisher, "Precision spectroscopy of $H_1 3CN$ using a free-running, all-fiber dual electro-optic frequency comb system," Opt. Lett. **43**(6), 1407–1410 (2018).
12. G. Millot, S. Pitois, M. Yan, T. Hovhannisyan, A. Bendahmane, T. W. Hänsch, and N. Picqué, "Frequency-agile dual-comb spectroscopy," Nat. Photonics **10**(1), 27–30 (2016).
13. T. Nishikawa, A. Ishizawa, M. Yan, H. Gotoh, T. Hänsch, and N. Picqué, "Broadband Dual-comb Spectroscopy with Cascaded-electro-optic-modulator-based Frequency Combs," in *Conference on Lasers and Electro-Optics (CLEO)* (Optica Publishing Group, 2015), paper SW3G.2.
14. L. Nitzsche, J. Goldschmidt, J. Kiessling, S. Wolf, F. Kühnemann, and J. Wöllenstein, "Tunable dual-comb spectrometer for mid-infrared trace gas analysis from 3 to 4.7 µm," Opt. Express **29**(16), 25449–25461 (2021).
15. S. Schiller, "Spectrometry with frequency combs," Opt. Lett. **27**(9), 766–768 (2002).
16. D. Bruneau, F. Gibert, P. Flamant, and J. Pelon, "Complementary study of differential absorption lidar optimization in direct and heterodyne detections," Appl. Opt. **45**(20), 4898–4908 (2006).
17. J. W. Goodman, "Statistical Properties of Laser Speckle Patterns," in *Laser Speckle and Related Phenomena* (Springer, 1975), Vol. 9.
18. G. Ehret, C. Kiemle, M. Wirth, A. Amediek, A. Fix, and S. Houweling, "Space-borne remote sensing of CO_2, CH_4, and N2O integrated path differential absorption lidar: a sensitivity analysis," Appl. Phys. B **90**(3-4), 593–608 (2008).
19. J. W. Goodman, "Statistical properties of laser speckle patterns," Technical Report No. 2303-1, Stanford Electronics Laboratories, Stanford University, (1963).
20. G. Parry, "The Scattering of Polychromatic Light from Rough Surfaces First Order Statistics," Opt. Quantum Electron. **7**(4), 311–318 (1975).
21. G. Parry, "Speckle Patterns in Partially Coherent Light," in *Laser Speckle and Related Phenomena* (Springer, 1975), Vol. 9.
22. E. MacKerrow, M. Schmitt, and D. Thompson, "Effect of speckle on lidar pulse–pair ratio statistics," Appl. Opt. **36**(33), 8650–8669 (1997).
23. G. Wagner and D. Plusquellic, "Ground-based, integrated path differential absorption LIDAR measurement of CO_2, CH_4, and H_2O near 1.6μm," Appl. Opt. **55**(23), 6292–6310 (2016).
24. B. Ruffing, "Application of speckle-correlation methods to surface-roughness measurement: a theoretical study," J. Opt. Soc. Am. A **3**(8), 1297–1304 (1986).
25. D. Léger, E. Mathieu, and J. Perrin, "Optical Surface Roughness Determination Using Speckle Correlation Technique," Appl. Opt. **14**(4), 872–877 (1975).